Ergodicity and scars of the quantum cat map in the semiclassical regime

Jiao Wang,[1,2] C.-H. Lai,[1] and Yan Gu[2]
[1]*Department of Physics, National University of Singapore, 10 Kent Ridge Crescent, Singapore 119260, Singapore*
[2]*Department of Astronomy and Applied Physics, University of Science and Technology of China, 230026 Hefei, Anhui, China*
(Received 9 March 2000; revised manuscript received 14 December 2000; published 17 April 2001)

We study the quantum localization effect of the cat map manifested in the motions of statistical ensembles. Specifically, the coarse-grained entropy and time-averaged phase space distributions are investigated. For this purpose, an amended version of the Wigner function on the discretized phase torus is presented. We find that the time average of the coarse-grained Wigner function is scarred (antiscarred) along some short periodic orbits, and the heights (depths) of these scars (antiscars) decrease in a linear way with the Planck constant when the semiclassical limit is approached. The relationship between the scars observed here and those exhibited in the quasienergy eigenstates is discussed.

DOI: 10.1103/PhysRevE.63.056208 PACS number(s): 05.45.−a

I. INTRODUCTION

Classically, ergodicity plays an important role in studying the random behaviors of dynamical systems. One fascinating problem is how it manifests itself in quantum mechanics, and in what way it is restored in the semiclassical limit ($\hbar \to 0$). A fundamental theorem by Schnirelman, together with those who came after him [1], has answered the basic aspect of the question; i.e., for a classically defined operator, its quantum expectations over almost all individual eigenstates converge to the ergodic, microcanonical averages of its classical counterpart as $\hbar \to 0$. Some authors also studied the rate at which they do so [2].

Later on, a lot of work was done in seeking the quantum characteristics possessed by the classically ergodic systems. One breakthrough was made in 1984 by Bohigas *et al.* [3], who conjectured that in the semiclassical limit the properties of the spectrum and the eigenstates of a chaotic system can be predicted based on the random matrix theory (RMT) [4]. This implies Gaussian random eigenfunctions and a strongly repulsive spectrum, whose concrete forms have a dependence on the symmetry properties of the system. The Gaussian random form of eigenfunctions implies marginally Schnirelman's ergodicity (for this reason, the ergodicity implied by the RMT is also known as ''strong quantum ergodicity'' while that in the sense of Schnirelman is known as ''weak quantum ergodicity'' [5]). The most striking point of this conjecture is that the RMT is only concerned with the overall symmetries of the system rather than any detailed dynamics. Hence the RMT's success in approximating some quantum descriptions of a chaotic system indicates clearly the leading role played by the symmetries in question. On the other hand, it is thus natural to expect that in more accurate approximations some dynamical aspects of the system should be taken into account as well. A well-known example is Gutzwiller's semiclassical trace formula [6], from which nonrandom fluctuations in the spectrum of a chaotic system can be connected to the short periodic orbits.

Short periodic orbits also have an important effect on the structure of the eigenstates of a chaotic system. This effect, termed ''scarring'' [7], is the anomalous enhancement or suppression of eigenstate intensity on or near an unstable periodic orbit and its invariant manifolds [8]. These enhanced or suppressed regions are called scars or antiscars [7,9]. They stand out against the monotonous background of the eigenstates derived from RMT and thus constitute the main correction to the latter. Generally they have a width of order $\hbar$; therefore, their existence would not destroy Schnirelman's ergodicity.

These important results regarding the quantum ergodicity mainly surround the properties of the spectrum and the individual eigenstates. However, to get a deeper insight into the classical-quantum correspondence of ergodicity, the properties involving many eigenstates at a time need to be studied as well. In fact, only for such properties does the classical-quantum correspondence have implications [5]. The reason lies in the essential difference between classical and quantum mechanics, from which a direct classical-quantum comparison of physical meaning is expected to be performed in the framework of statistical mechanics.

In most cases, however, it would be a very difficult job to cope with the statistical ensembles of a chaotic system. The situation becomes even harder when the deep semiclassical limit and long time evolutions need to be considered. As a result, our knowledge in this regard is still quite limited. For example, an immediate question one would want answered is whether an even phase-space distribution will be converged to by a general quantum ensemble apart from the inevitable quantum fluctuations, and if not, whether the phase space will be evenly visited in the sense of time average. This question will be focused on in this paper.

The model system we adopt is Arnold's cat map [10], a well-known paradigm of classical chaos. It turns out to be ideal for our plan here due to its generality and simplicity. Specifically, by using the quantum characteristic function [11], its evolution equation can be transformed into a much simpler one, which has been proven to be crucial for both analytic and numerical work [12,13], especially related to the motions of ensembles. If the coarse-graining procedure is involved, this new form evolution equation will allow further simplification of the calculations. Quantum characteristic functions, as shown in this paper, are also important for defining a new Wigner function for the system whose phase space is a torus like the cat map.

We find that a very interesting quantum localization effect may appear during the evolutions of a wave packet. After the initial relaxation period, the phase space would be evenly distributed up to the randomlike quantum fluctuations in most cases; but surprisingly, at other times some strongly localized structures caused by quantum interference, whose scales are of the same order of the initial wave packet, would emerge from this monotonous background. This is in contrast with the classical mixing property. In addition, if the Plank constant is decreased (being divided by a prime number repeatedly), these structures themselves are kept completely unchanged (except for the times at which they appear may change greatly). This is different from the dynamical localization effect [14,15] which does not survive the semiclassical limit. However, since the average interval between the appearances of these localized structures increases as $\hbar \to 0$, the time-averaged phase-space distribution will finally reach that required by the classical ergodicity in the semiclassical limit.

Another interesting phenomenon is that when the initial wave packet is launched on or near a periodic orbit, it is found along not only that one, but also some other periodic orbits in which the time-averaged phase space distribution protrudes. This suggests that to understand the scars along a given periodic orbit, it is insufficient to consider only the information contained in the dynamics of the wave-packet origins from this single periodic orbit; the information contained in the wave-packet dynamics along other periodic orbits must be considered as well. This implies that the scarring should be seen as a collective effect to which various periodic orbits make their contributions simultaneously in some inseparable way.

This paper is organized as follows. In the next section, we first discuss briefly the quantization of the cat map, and then we introduce the quantum characteristic function, which is equivalent to the density operator in describing a quantum ensemble. In terms of this, a simple evolution formula for the quantum cat map is derived. Section III presents a new definition of the Wigner function for the system whose phase space is a torus, and its propagator for Arnold's cat map is discussed. The quantum interference exhibited in the motions of an ensemble can be illustrated by simply examining this propagator. Section IV discusses the coarse-graining procedure, and Sec. V presents the numerical results. In Sec. VI, we discuss the semiclassical behavior of the time average of the coarse-grained Wigner function and the relationship between the scars exhibited in this presentation and those exhibited in the quasienergy eigenfunctions. A concise summary will be found in the final section.

II. QUANTIZATION OF THE CAT MAP

To quantize the cat map, several schemes are currently available [16–18]. Among them, a general method for quantizing a linear map on the torus has been studied in detail by Hannay and Berry [16]. But unfortunately, our model system does not satisfy the conditions of their formulation. Another scheme, which we shall resort to here, is that once discussed by Balazs and Voros in their study of Baker's transformation [17]. It consists of two steps. The first one is to specify the kinematics, i.e., the states and the operators that are involved in the description of the system; and the second is to construct the dynamics, i.e., the time evolution operator that acts on them. The latter step can be carried out by a direct analogy with the classical dynamics.

Assume the phase space is a torus with unit area. The fact that it is compact implies that the number of phase cells $N=1/(2\pi\hbar)$ is a finite integer that gives the dimension of the state-vector space needed to describe the system. We denote such an N-dimensional Hilbert space as $\mathcal{H}$, and construct two orthogonal, complete vector sets $\{|j\rangle\}$ and $\{|\overline{l}\rangle\}$ with $j,l=0,\ldots,N-1$. They are assumed to be related by the following transformations:

$$|\overline{l}\rangle=\frac{1}{\sqrt{N}}\sum_{j=0}^{N-1} e^{i2\pi jl/N}|j\rangle, \tag{2.1a}$$

$$|j\rangle=\frac{1}{\sqrt{N}}\sum_{l=0}^{N-1} e^{-i2\pi jl/N}|\overline{l}\rangle. \tag{2.1b}$$

Then, the position and momentum operators $\hat{q}$ and $\hat{p}$ can be defined as the eigenoperators of these two vector sets, respectively, by

$$\hat{q}|j\rangle=\frac{j}{N}|j\rangle, \quad j=0,\ldots,N-1, \tag{2.2a}$$

$$\hat{p}|\overline{l}\rangle=\frac{l}{N}|\overline{l}\rangle, \quad l=0,\ldots,N-1. \tag{2.2b}$$

It is worth noting that the operator pair $\hat{q},\hat{p}$ thus defined does not obey the Heisenberg commutation rule but rather the following Weyl commutation rule [19]:

$$e^{i2\pi n\hat{p}}e^{i2\pi m\hat{q}}=e^{i2\pi mn/N}e^{i2\pi m\hat{q}}e^{i2\pi n\hat{p}}, \quad (m,n)\in\mathcal{Z}^2. \tag{2.3}$$

As to the dynamics of a density operator $\hat{\rho}$, if the unitary time evolution operator $\hat{S}$ corresponding to the classical map has been obtained in some way, then the time evolution of $\hat{\rho}$ can be described by

$$\hat{\rho}^{k+1}=\hat{S}\hat{\rho}^{k}\hat{S}^{\dagger}, \tag{2.4}$$

where k and $k+1$ represent two successive integral times. Obviously, it would be difficult in practice to evolve the quantum ensemble by using this formula directly, especially for the cases in which N is large. To facilitate the calculation, a key technique used in this paper is to make good use of the quantum characteristic function of the density operator $\hat{\rho}$, which is defined as [11–13]

$$\varphi(m,n)=\mathrm{Tr}[\hat{\rho}\hat{U}(m,n)], \quad (m,n)\in\mathcal{Z}^2, \tag{2.5}$$

where $\hat{U}(m,n)=e^{i\pi mn/N}e^{i2\pi m\hat{q}}e^{i2\pi n\hat{p}}$ acts as a phase-space displacement operator, i.e.,

$$\hat{U}(m,n)|j\rangle = e^{i\pi m(2j-n)/N}|[j-n]_N\rangle, \tag{2.6a}$$

$$\hat{U}(m,n)|\overline{l}\rangle = e^{i\pi n(2l+m)/N}|\overline{[l+m]_N}\rangle. \tag{2.6b}$$

Here $[\,]_N$ denotes the congruence modulo N. It is easy to verify that the symmetries of $\hat{U}(m,n)$,

$$\hat{U}(m+N,n) = (-1)^n \hat{U}(m,n),$$

$$\hat{U}(m,n+N) = (-1)^m \hat{U}(m,n), \tag{2.7a}$$

$$\hat{U}^\dagger(m,n) = \hat{U}(-m,-n) \tag{2.7b}$$

can be passed on to the quantum characteristic function $\varphi(m,n)$, i.e.,

$$\varphi(m+N,n) = (-1)^n \varphi(m,n),$$

$$\varphi(m,n+N) = (-1)^m \varphi(m,n), \tag{2.8a}$$

$$\varphi^\star(m,n) = \varphi(-m,-n). \tag{2.8b}$$

From Eq. (2.8a), one realizes that although $\varphi(m,n)$ has a period of $2N$ for both m and n, only N^2 values on a square $N\times N$ lattice are independent. This can also be verified directly by the inverse transformation between the density operator and its quantum characteristic function,

$$\hat{\rho} = \frac{1}{N} \sum_{m=m_0}^{m_0+N-1} \sum_{n=n_0}^{n_0+N-1} \varphi(m,n)\hat{U}^\dagger(m,n). \tag{2.9}$$

This means that the characteristic function $\varphi(m,n)$ on an arbitrary $N\times N$ square lattice can completely describe a quantum ensemble (m_0 and n_0 are two arbitrarily chosen integers). We emphasize this fact because it is crucially important for our later discussions on the Wigner function.

Now let us turn to the cat map. The classical dynamics of the cat map can be derived from the model of a periodically kicked one-dimensional particle with unit mass and it has the Hamiltonian [18]

$$H = \frac{1}{2}p^2 + \frac{K}{2}q^2\delta_1(t), \tag{2.10}$$

where $\delta_1(t)$ represents a sequence of δ functions with period of unit time. Integrating the equations of motion derived from this Hamiltonian over a unit time from just before the kth kick to just before the $(k+1)$th kick, and imposing periodic boundary conditions to both q and p to make the phase space a unit torus, one obtains

$$\begin{pmatrix} q_{k+1} \\ p_{k+1} \end{pmatrix} = \begin{pmatrix} 1-K & 1 \\ -K & 1 \end{pmatrix} \begin{pmatrix} q_k \\ p_k \end{pmatrix} \pmod 1. \tag{2.11}$$

If $|K-2|>2$, this map is an Anosov diffeomorphism on a 2-torus. The motion generated by such a map is strongly chaotic, and in particular is mixing and ergodic. The Arnold cat map that we address later corresponds to $K=-1$ [10].

From the quantum counterpart of the Hamiltonian given above, the unitary time evolution operator corresponding to the classical map can be integrated out exactly, which yields

$$\hat{S} = e^{-i\pi N\hat{p}^2} e^{-i\pi NK\hat{q}^2} \tag{2.12}$$

with two factors being responsible for the kick and the free motion between two successive kicks, respectively. After a straightforward calculation by using Eq. (2.4), the time evolution of the quantum characteristic function generated by this unitary evolution operator can be given by

$$\varphi^{k+1}(m_{k+1},n_{k+1}) = \varphi^k(m_k,n_k) \tag{2.13}$$

with

$$\begin{pmatrix} m_{k+1} \\ n_{k+1} \end{pmatrix} = \begin{pmatrix} 1 & K \\ -1 & 1-K \end{pmatrix} \begin{pmatrix} m_k \\ n_k \end{pmatrix} \tag{2.14}$$

for even N, which is the case being dealt with in this paper. Due to the periodic conditions (2.8a), the iteration formulas (2.13) and (2.14) can be constrained on any $2N\times 2N$ square lattice. Since $\varphi(m,n)$ is actually permuted on this finite lattice, it must return to its initial state after a finite number of iterations. This period, denoted in this paper by $\alpha(N)$, is known as the quantum period of the system [16]. Research reveals that $\alpha(N)$ has a strong dependence on the number-theoretical nature of N [20].

Comparing with Eq. (2.4), the evolution formulas (2.13) and (2.14) have an apparent advantage in that only integral operations are involved. Consequently, much less memory and time are needed when the numerical calculations are implemented. This is one of the reasons why we resort to the quantum characteristic function in our investigations. In Sec. IV, one may find that, based on these two formulas, the numerical calculations can be simplified further as a consequence of coarse-graining.

III. WIGNER FUNCTION

The Wigner function is one of the most useful tools to investigate the motion of a quantum ensemble in phase space. In this section, we will present an appropriate definition of the Wigner function for the systems whose kinematics were constructed in the preceding section.

From its conventional definition, a straightforward Wigner function for the linear quantum maps on a two dimensional torus has been given by Hannay and Berry (HB) [16]. It has period 1 in both the q and p directions, and nonzero values on a $2N\times 2N$ lattice in the phase torus. In fact, this Wigner function, referred to as $W_{\rm HB}(q,p)$ in the following, can be expressed as the Fourier transformation of the quantum characteristic function on a $2N\times 2N$ square lattice in the Fourier dual space of the torus, i.e.,

$$W_{\rm HB}(q_j,p_l) = \frac{1}{4N^2} \sum_{m,n=0}^{2N-1} \varphi(m,n) e^{-i2\pi(mq_j+np_l)} \tag{3.1}$$

with $(q_j,p_l) = (j/2N, l/2N)$, $(j,l)\in \mathcal{Z}^2$. From Eq. (2.8a), we know that, for $4N^2$ terms of $\varphi(m,n)$ appearing in the right-

hand side of this definition, only N^2 of them are independent; this infers that $4N^2$ spikes of $W_{\mathrm{HB}}(q_j,p_l)$ on the phase torus are associated in sets of four as already having been pointed out by Hannay and Berry [16]. This is in fact a shortcoming, because those redundant spikes cannot provide any new information, and even worse, they make the physical meaning of the Wigner function too vague to understand [17].

As suggested by Eq. (2.9), a quantum characteristic function defined on an $N\times N$ square lattice is sufficient for describing a quantum ensemble. This fact implies that it is the superfluous terms of $\varphi(m,n)$ in definition (3.1) that cause the trouble, and therefore it is preferable to carry out the summation in the right-hand side of Eq. (3.1) only within an $N\times N$ square lattice (denoted as Λ) in the Fourier dual space instead. This consideration leads straightforwardly to a redefined Wigner function,

$$W(q_j,p_l)=\frac{1}{N^2}\sum_{(m,n)\in\Lambda}\varphi(m,n)e^{-i2\pi(mq_j+np_l)}. \quad (3.2)$$

Obviously, this new version of the Wigner function defined here contains all the necessary information needed to specify a quantum ensemble, and therefore it can serve as a complete description of it. In addition, one can easily deduce that it has the projection nature

$$\sum_{l=0}^{N-1}W(q_j,p_l)=\langle j|\hat{\rho}|j\rangle,\quad j=0,\ldots,N-1, \quad (3.3a)$$

$$\sum_{j=0}^{N-1}W(q_j,p_l)=\langle\overline{l}|\hat{\rho}|\overline{l}\rangle,\quad l=0,\ldots,N-1 \quad (3.3b)$$

expected for a Wigner function. This further supports the validity of the new definition. Periodic conditions

$$W(q_j+1,p_l)=W(q_j,p_l+1)=W(q_j,p_l) \quad (3.4)$$

are satisfied as well, and as a result (q_j,p_l) can be restricted on the $N\times N$ phase lattice $\{(q_j,p_l)=(j/N,l/N);\ j,l=0,\ldots,N-1\}$, which will be referred to as the Wigner lattice in the following.

Compared with its conventional version (3.1), the advantage of this redefined Wigner function is that the redundant phase-space points that are not required by the position or momentum wave-function descriptions are no longer involved. The Wigner lattice can therefore be viewed as the quantum counterpart to the classical phase torus. This fact makes the physical meaning of this definition more clear.

On the other hand, from Eq. (2.8b) one knows that $W(q_j,p_l)$ is real if the $N\times N$ lattice Λ is symmetric about the origin. Therefore, for odd N one can generate a real $W(q_j,p_l)$ by just specifying the Λ used in Eq. (3.2) as the symmetric one whose lower left vertex is located at $(-(N-1)/2,-(N-1)/2)$. But for even N, this effort fails and thus $W(q_j,p_l)$ is in general complex. A better choice in this case is to locate the lower left vertex of Λ at $(-N/2,-N/2)$, so that the image part of $W(q_j,p_l)$ only comes from the contributions of those terms of $\varphi(m,n)$ along the left and the lower edges of Λ. However, since in both cases the values of $W(q_j,p_l)$ are not non-negative–definite, $W(q_j,p_l)$ cannot serve as a phase space probability distribution directly. As far as this point is concerned, our viewpoint is that being real but possibly negative (odd N) is by no means better than being complex (even N). Fortunately, it turns out that this defect of $W(q_j,p_l)$ can be remedied by coarse-graining it in some appropriate ways. For example, the corresponding Husimi distribution of $W(q_j,p_l)$ is found to be actually everywhere nonnegative for both odd and even N, at least under the condition $N\gg 1$, as we will show in the next section.

In the rest of this section, we would like to give the explicit expression of the one-step propagator of this newly defined Wigner function for Arnold's cat map ($K=-1$). For the conventional Wigner function, the study by Hannay and Berry has revealed that for a linear map, W_{HB} is just carried along by the classical map on a $2N\times 2N$ phase lattice, and no quantum effect is found to be manifested explicitly in this simple picture. In contrast, the following results will show that the propagation of $W(q_j,p_l)$ seems to be more complicated and exhibits impressive quantum effects.

Assume that after one evolution step the Wigner function can be expressed as

$$W^{k+1}(q_{j'},p_{l'})=\sum_{j,l=0}^{N-1}W^k(q_j,p_l)P(q_{j'},p_{l'};q_j,p_l), \quad (3.5)$$

where $P(q_{j'},p_{l'};q_j,p_l)$ represents the contribution of the spike located at (q_j,p_l) to that at $(q_{j'},p_{l'})$ after one iteration; then by substituting Eq. (3.2) into both sides of this equation and by making use of Eqs. (2.13) and (2.14), one obtains

$$P(q_{j'},p_{l'};q_j,p_l)=\frac{1}{N^2}\sum_{(m,n)\in\Lambda}\lambda(m,n)e^{i2\pi[m(q_j-q_{j'}+p_{l'})+n(p_l-2p_{l'}+q_{j'})]} \quad (3.6)$$

with

$$\lambda(m,n)=\begin{cases}(-1)^{m+n} & \text{if} \quad n-s\leqslant m\leqslant 2n-s \quad \text{or} \quad 2n+s<m<n+s;\\ (-1)^n & \text{if} \quad n>m+s \quad \text{or} \quad n\leqslant m-s; \qquad \left(s=\dfrac{N}{2}\right)\\ 1 & \text{if} \quad 2n-s<m\leqslant 2n+s.\end{cases} \quad (3.7)$$

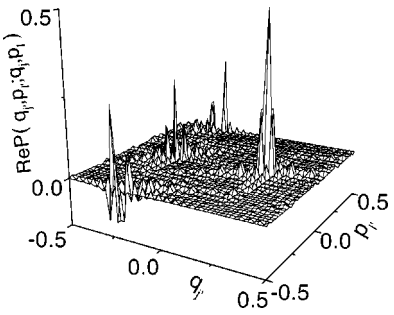

FIG. 1. The real part of the one-step propagator of the Wigner function for the cat map with $N=48$. The initial spike is at $(q_j,p_l)=(0.25,-0.25)$.

In Fig. 1, we show for $N=48$ and $(q_j,p_l)=(0.25,-0.25)$ the real part of the function $P(q_{j'},p_{l'};q_j,p_l)$ as an example to see how a spike fixed at (q_j,p_l) will be propagated on the Wigner lattice (please note that the origin of the phase space is located at the center in this figure and in all subsequent figures in which phase space is concerned). Since the maximum of the imaginary part is quite small compared with that of the real part (0.02 versus 0.5), Fig. 1 reflects almost all the main details of the propagator.

In this figure, we can see three prominent peaks situated exactly on three vertices of a right triangle whose two right sides are parallel to the axes and have the same length of 0.5. The highest peak has a strength of 0.5, and its location (0.25,0) is exactly where (q_j,p_l) would be mapped under the classical map. The other two lower peaks, having the same height of 0.25, are situated at $(-0.25,0)$ and $(-0.25,-0.5)$, respectively; they have no classical analog and are thus responsible for the quantum character of the cat map. Straightforward analysis shows that if (q_j,p_l) is shifted, the pattern of $P(q_{j'},p_{l'};q_j,p_l)$ will not change but will suffer a corresponding displacement.

Further investigations of Fig. 1 reveal that there are many deep valleys in the immediate neighborhood of two nonclassical peaks, which lead to noticeable fluctuation structures. The wavelength of these structures is of order $\hbar$. Since the Wigner function of a wave packet has a minimum width of order $\sqrt{\hbar}$, the nonclassical contributions from neighboring points will counterbalance each other greatly during the initial evolving stage. This explains why the propagation of a wave packet resembles that of the corresponding classical phase density before the quantum coherence appears [21].

IV. COARSE-GRAINING

As was illustrated in the preceding section, the Wigner function itself is generally not non-negative-definite. In order to appreciate its real significance, one has to resort to its coarse-grained form to obtain an appropriate phase-space representation. On the other hand, since coarse-graining would smooth out all high wave-number undulations, this procedure makes it possible for various phase-space structures specific to the quantum motions to manifest themselves in a clear way. In addition, as fewer wave numbers are involved, time and memory used in the numerical calculations can be reduced further.

For simplicity, we use a Gaussian coarse-graining factor and denote its width by ϵ with $\sqrt{\hbar}\leqslant\epsilon\ll 1$. Then the coarse-grained Wigner function can be written as

$$W_\epsilon(q_j,p_l)=C\sum_{j',l'=-\infty}^{\infty} e^{-[(q_{j'}-q_j)^2+(p_{l'}-p_l)^2]/\epsilon^2}W(q_{j'},p_{l'}), \tag{4.1}$$

where C is an appropriate normalizing factor. However, in practical calculations, it is more convenient to express W_ϵ in terms of the quantum characteristic function

$$W_\epsilon(q_j,p_l)=\frac{1}{N^2}\sum_{(m,n)\in\Lambda}\varphi_\epsilon(m,n)e^{-i2\pi(mq_j+np_l)} \tag{4.2}$$

and resort to the approximate relation [13]

$$\varphi_\epsilon(m,n)\approx e^{-\pi^2\epsilon^2(m^2+n^2)}\varphi(m,n) \quad \text{for}$$
$$(m,n)\in\Lambda, \quad N\epsilon\gg 1. \tag{4.3}$$

The Gaussian coarse-graining factor appearing in this equation acts as a wave filter, which causes the value of $\varphi_\epsilon(m,n)$ to be negligible for (m,n) outside a smaller central region of Λ whose radius depends only on the coarse-graining size ϵ and does not grow as N is increased. As a consequence, the summation on the right-hand side of Eq. (4.2) can be carried out only within this region, which provides an essential simplification to the numerical calculations, especially when large N (or the deep semiclassical limit) has to be dealt with.

Now we show that when $N\gg 1$ and $\epsilon\geqslant\sqrt{\hbar}$, $W_\epsilon(q_j,p_l)$ is essentially everywhere non-negative. Letting $|j\rangle\equiv|[j]_N\rangle$, $j\in\mathcal{Z}$; when $N\gg 1$, we may define a coherent state centered at (q_j,p_l) as

$$|\psi\rangle=\left(\frac{2}{N}\right)^{1/4}\sum_{j'=-\infty}^{\infty} e^{-\pi[(j'-j)^2-i2l(j'-j)]/N}|j'\rangle. \tag{4.4}$$

Its Wigner function has the form

$$W^\psi(q_{j'},p_{l'})=\frac{2}{N}e^{-2\pi N[(q_j-q_{j'})^2+(p_l-p_{l'})^2]}. \tag{4.5}$$

Substituting it into Eq. (4.1) and letting $\epsilon=\sqrt{\hbar}$, we have

$$W_{\sqrt{\hbar}}(q_j,p_l)=\sum_{j',l'=-\infty}^{\infty}W^\psi(q_{j'},p_{l'})W(q_{j'},p_{l'})$$
$$=\frac{1}{N}\langle\psi|\hat{\rho}|\psi\rangle$$
$$\geqslant 0. \tag{4.6}$$

Here $W_{\sqrt{\hbar}}$ is actually the Husimi distribution of the density operator $\hat{\rho}$ [22].

Having appropriately defined a phase-space distribution, we are now in a position to study the phase-space structures imprinted by the quantum motions, which is expected to reveal the localization effect of the quantum chaos caused by quantum coherence. We will use a Gaussian wave packet as a probe and locate its centroid at various positions of interest (e.g., near or on a particular classical periodic orbit) to study how the long-time behavior of a quantum ensemble is influenced by the corresponding classical phase-space structures. The quantum characteristic function for such an initial Wigner function has the form

$$\varphi^0(m,n)=e^{i2\pi(mq_j+np_l)}e^{-a^2\pi^2(m^2+n^2)} \quad \text{for}$$

$$(m,n)\in\Lambda, \quad N\gg 1. \tag{4.7}$$

Here (q_j,p_l) is the center position of the probe in phase space and a is its width in both q and p coordinates.

Our numerical investigations on the localization effect of the quantum cat map consist of two parts. We will first focus our attention on the time evolution of the coarse-grained entropy. In order to facilitate the numerical calculations, a different expression for nonequilibrim entropy $S=-K_B\ln(\mathrm{Tr}[\hat{\rho}^2])$, which was first suggested by Prigogine [23], is used. Setting the Boltzmann constant $K_B=1$, the coarse-grained entropy of a quantum ensemble of a cat map is [13]

$$S_\epsilon=-\ln\left(\sum_{(m,n)\in\Lambda}|\varphi_\epsilon(m,n)|^2\right)$$

$$=-\ln\left(\sum_{j,l=0}^{N-1}|W_\epsilon(q_j,p_l)|^2\right)-2\ln N. \tag{4.8}$$

Besides that, we will also study the phase-space structures left by a wave packet during its evolutions by calculating the time average of the coarse-grained Wigner function over the whole quantum period, i.e.,

$$\overline{W}_\epsilon(q_j,p_l)=\frac{1}{\alpha(N)}\sum_{k=0}^{\alpha(N)-1}W_\epsilon^k(q_j,p_l). \tag{4.9}$$

V. NUMERICAL RESULTS

A. Quantum coarse-grained entropy (QCE)

In this subsection, we show some of the numerical results of the time evolutions of the coarse-grained entropy and study its semiclassical behavior. By using the periodic conditions (2.8a) and the recurrence formulas (2.13) and (2.14), the QCE at time k can be expressed as

$$S_\epsilon^k=-\ln\left(\sum_{(m_0,n_0)\in\Lambda}e^{-2\epsilon^2\pi^2([m_k]^2+[n_k]^2)}|\varphi^0(m_0,n_0)|^2\right), \tag{5.1}$$

where $([m_k],[n_k])\in\Lambda$, $[m_k]=m_k$, and $[n_k]=n_k(\mathrm{mod}\,N)$. In Fig. 2, we show several time curves of QCE for $\epsilon=0.000\,04$ and $N=10^5$, 10^6, and 4×10^6, respectively. The initial phase-space distribution, whose quantum characteristic function has the form of Eq. (4.7) with $a=0.001\,261\,6$ (noting that for the case $N=10^5$ we have $a=\sqrt{\hbar}$, which means that the initial distribution describes a coherent state), is Gaussian. The evolution of the corresponding classical coarse-grained entropy is also shown.

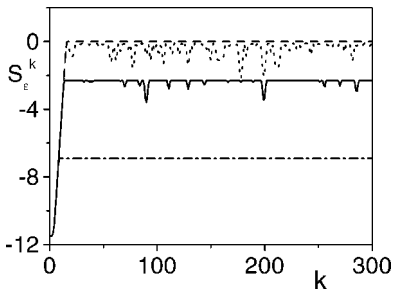

FIG. 2. Coarse-grained entropy for the quantum cat map. The initial Gaussian distribution is centered at (0,0) with $a=0.001\,261\,6$, $\epsilon=0.000\,04$, and $N=10^5$ (dot-dash line), 10^6 (solid line), and 4×10^6 (dotted line). The dashed line gives its classical counterpart.

In this figure, we can see that the time evolution of the QCE undergoes two stages. In the relaxation stage, it increases in the same way as its classical analog does, and the ascending trend will not stop until a critical entropy value is approached. After that moment, however, while the classical coarse-grained entropy goes on increasing up to the equilibrium S_{eq} and stays there invariably, the QCE stops increasing and begins to show an irregular sequence of dips of different sizes thereafter.

The appearance of the dip sequence caused by quantum coherence in the time curve of QCE after the relaxation stage reveals a significant difference between the quantum motions and the classical mixing dynamics. In order to show clearly how this difference disappears as the quantum motion approaches its classical limit, we use the time-averaged deviation of the QCE from that of its classical counterpart $\Delta S=S_{\mathrm{eq}}-\overline{S_\epsilon}$ as a measure and investigate its semiclassical behavior. As we do so, we find that for fixed initial phase-space distributions, the entropy difference ΔS exhibits a strong dependence on the number-theoretical nature of N, just like many other characters of the quantized cat map have shown [20]. In order to reveal the trend of ΔS in the semiclassical limit that underlies these number-theoretical fluctuations, a natural method is to smooth the curve (ΔS versus N) out by averaging ΔS over a certain neighboring range of N for every sample point that resides on it, as was done in Ref. [13]. Here we would like to point out that these number-theoretical fluctuations can also be eliminated if one restricts the investigation along some specified sequences of N. Such a sequence can be generated by simply multiplying a positive integer N_0 with a prime b successively, i.e., $N_l=N_0b^l$, $l=1,2,\ldots$. In Table I, we show the sequence of ΔS_{N_l} for an initial Gaussian distribution with width $a=0.05$, and from it we find that as l increases, ΔS_{N_l} descends linearly with l^{-1}, i.e., $\Delta S\propto\hbar$ (this result is somewhat different from that we obtained by averaging ΔS over N, which indicates $\Delta S\propto\hbar^{0.72}$ [13]).

TABLE I. The dependence on Planck's constant $h=1/N$ of the deviation of the time-averaged quantum coarse-grained entropy and the time-averaged coarse-grained Wigner function from their classical counterparts. Initial Gaussian distribution is located at (0,0) with $a=0.05$, $\epsilon=0.035$. Three sample points on the phase torus used for evaluating $\Delta\overline{\mathcal{W}}(q,p)$ are (0,0), $(-0.5,-0.5)$, and (0.2,0.2).

N	$\alpha(N)$	ΔS	$\Delta\overline{\mathcal{W}}(0,0)$	$\Delta\overline{\mathcal{W}}(-0.5,-0.5)$	$\Delta\overline{\mathcal{W}}(0.2,0.2)$
300	300	0.24091	1.93061	−0.05909	−0.10665
600	300	0.19428	1.68646	−0.11526	−0.10534
1200	300	0.17525	1.57584	−0.10074	−0.08977
2400	600	0.11365	0.93976	0.10147	−0.06217
4800	1200	0.06089	0.49055	0.07140	−0.02984
9600	2400	0.03052	0.24642	0.03686	−0.01532
19200	4800	0.01526	0.12321	0.01843	−0.00766

Furthermore, we find for large enough l that all the dips in the time curve of QCE will be found to appear again in the next curve with a larger value of l, with only the times at which they appear undergoing a change. More interesting, the identified dips appearing in different time curves of QCE share the same phase-space distributions, too. On the other hand, no new dips are found to emerge as l increases further, hence the result observed above can be ascribed to the linear dependence of the quantum period on l when l is large enough (Table I).

B. Scars and antiscars in phase space

By using the coarse-grained Wigner function discussed above, we can conveniently investigate the motion of any ensemble in which we are interested in the phase space. One observation of interest is how an initial Gaussian distribution (IGD) evolves in the phase-space. Such an observation first appeared in Ref. [18] with a differently defined phase space distribution, and it impressed us due to the recurrence of the initial distribution as well as the complicated phase space structure exhibited in the transient equilibrium stage during a quantum period. In order to figure out the quantum localization nature of the cat map, we will focus our attention here on the time average of the coarse-grained Wigner function $\overline{W}_\epsilon(q_j,p_l)$ instead. Since it is defined on the discretized phase torus, for the purpose of illustrating the quantum-classical analogy, it is preferable to introduce a density distribution $\mathcal{W}(q,p)$ on the entire torus, which is uniform on each phase cell and is related to the coarse-grained Wigner function on the discretized phase torus by

$$\mathcal{W}(q_j,p_l)=N^2W_\epsilon(q_j,p_l). \tag{5.2}$$

As the equilibrium distribution on the phase torus is now expressed as $\mathcal{W}_{\rm eq}(q,p)=1$, our attention will be focused on the time-averaged quantity $\Delta\overline{\mathcal{W}}(q,p)=\overline{\mathcal{W}}(q,p)-1$, which could reflect the deviation from the classical ergodicity. A lot of patterns of $\overline{\mathcal{W}}$ with different N and different IGD for the Arnold cat map have been investigated. Although major patterns of $\overline{\mathcal{W}}$ resulting from the numerical calculations display complicated phase-space structures, we are able to recognize them as a superposition of two basic patterns, i.e., the imprints of the initial distribution and the quantum scars (antiscars). In the following, we shall describe the interesting features of these two types of patterns in detail.

1. The imprints of the initial distribution (IOID)

Since the motion of the quantum cat map is periodic, it is natural to expect IOID in the time-averaged phase-space distribution, especially when the quantum period $\alpha(N)$ is not too large. In Fig. 3, some typical patterns of IOID with Gaussian initial distributions are shown. Figures 3(a) and 3(b) are for a three-dimensional plot of $\overline{\mathcal{W}}$ and its contours, respectively, with $N=3998$, $\alpha(N)=333$. The IGD is centered at (0,0), which is the fixed point of the classical map. From these two figures, a prominent peak at the fixed point can be found, and away from this point, $\overline{\mathcal{W}}$ remains high along its stable and unstable manifolds. There is a simple argument that explains this phenomenon. In fact, the motion of a quantum ensemble is similar to that of its classical counterpart before the characteristic logarithmic time is reached [21]. During this stage, the IGD is squeezed along the stable manifold and stretched along the unstable manifold, and this effect would cause a considerable accumulation of $\overline{\mathcal{W}}$ along the unstable manifold as well as at the fixed point. This is also what happens to the stable manifold just before a quantum period elapses, but in the reverse time order. It is evident that such a mechanism is also effective in cases in which the IGD is located at other places. Noting that the time-averaged Wigner distribution is just a linear combination of the Wigner functions of the quasienergy eigenstates (see Sec. VI), this argument provides also a guide to the interpretation of the same phenomenon that has been observed in the study of the scars that appear in the eigenstates [24].

When the IGD is moved away from the fixed point, the patterns of IOID change accordingly. Figure 3(c) shows the contours of $\overline{\mathcal{W}}$ when the center of the initial Gaussian is moved to an arbitrarily chosen point $(-1/6,-22/153)$. In this plot, besides the peak at the initial point, one can find clearly the imprints left by the first three iterations as well as that left by the last three iterations before the ensemble distribution returns to its initial state. In our numerical calculations, we also found another type of IOID that appears only when the motion of the quantum cat has an even period. For such quantum cats, the initial distribution may reappear after the half-quantum period at its symmetrical position with respect to the origin (0,0). Figure 3(d) shows an example of this type of IOID when the initial Gaussian is located at $(-1/6,-22/153)$ with $N=2554$ and $\alpha(N)=426$.

2. Scars and antiscars

Apart from the above-mentioned IOID, most patterns of $\overline{\mathcal{W}}$ may actually display additional peaks and dips along some classical short periodic orbits. These phase-space structures are caused by the quantum coherence during the equilibrium stage [18,13] and could be recognized as scars and antiscars (here the readers should not be confused with the examples shown in Fig. 3, which happen to be those in

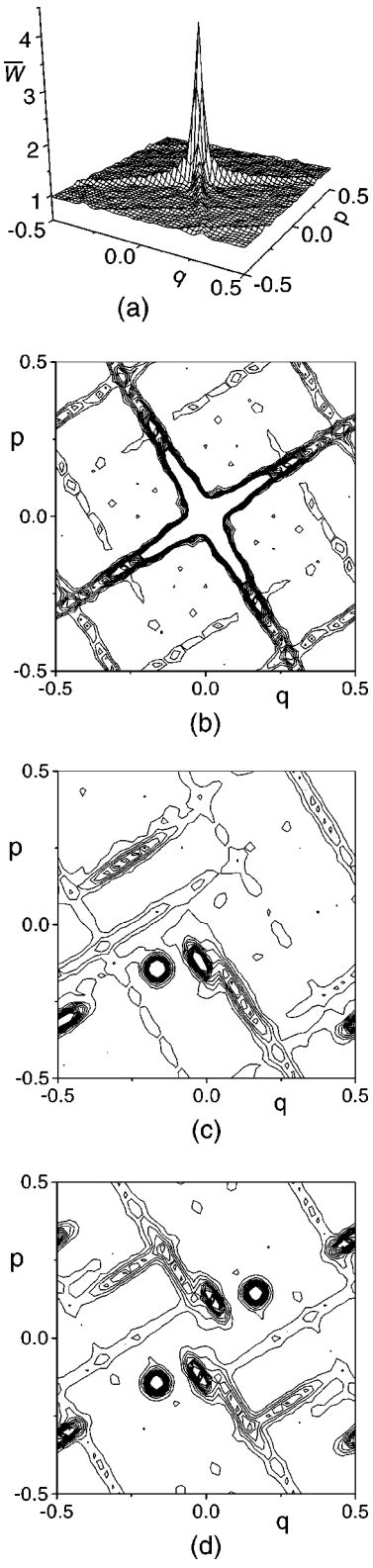

FIG. 3. Time-averaged ensemble density distributions $\overline{\mathcal{W}}(q,p)$ with $a=0.024$ and $\epsilon=0.021$. (a) A three-dimensional plot for $N=3998$ [$\alpha(N)=333$] and IGD at (0,0). (b) The contours for $\overline{\mathcal{W}}$ shown in (a) ranging from 0.99 to 1.09 with space 0.0125. (c) and (d) Contours of $\overline{\mathcal{W}}$ from 1 to 1.4 (spacing size 0.04) for the IGD at $(-1/6,-22/153)$ with $N=3998$ and $N=2554$ [$\alpha(N)=426$], respectively.

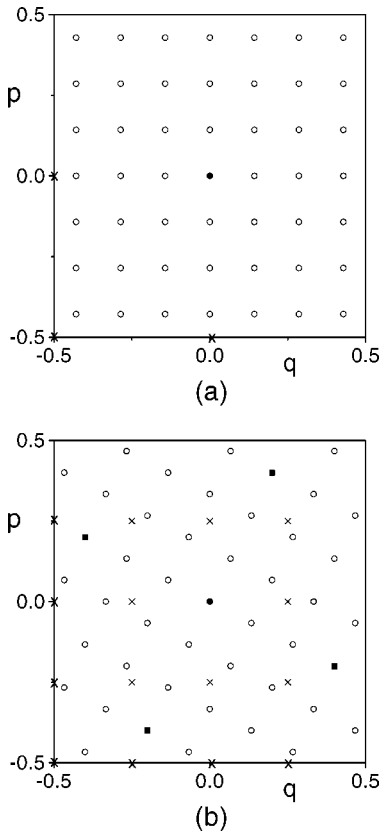

FIG. 4. (a) Two invariant sublattices for $N=686$: I_1 (dot and crosses) and I_2 (dot and circles). (b) Periodic orbits of the cat map up to period 4. Dot for the fixed point, squares for two period-2, crosses for four period-3, and circles for ten period-4 orbits, respectively.

which these structures are greatly depressed and hence are ideal for illustrating the IOID). Although it is not an easy task to determine exactly whether a certain classical orbit will be scarred or not under the given conditions, some simple rules are strongly suggested by the numerical data. For example, one of our findings is that when the IGD is located at the fixed point, all of the scarred classical periodic orbits will be exactly organized to form some of the invariant sublattices of the Wigner lattice. It is interesting to note that the concept of an invariant sublattice plays an important role also in the mathematical study of the classical periodic orbits of the cat map by using the ideal theory in quadratic fields [25]. For the convenience of the following illustrations, in Fig. 4(a) two invariant sublattices of the Wigner lattice for $N=686$ are plotted. They are $I_1=\{(q,p)|q=j/2,\ p=l/2,\ j,l=-1,0\}$ and $I_2=\{(q,p)|q=j/7,\ p=l/7,\ j,l=-3,\ldots,3\}$, respectively. The former consists of the fixed point and a period-3 orbit that passes through $(-0.5,-0.5)$ (denoted as O_1), while the latter consists of the fixed point and six period-8 orbits.

In Fig. 5(a), we show a three-dimensional plot of $\overline{\mathcal{W}}$ for $N=686$, $\alpha(N)=1176$ with $a=0.024$, $\epsilon=0.021$. The IGD is centered at the fixed point (0,0). In this plot, besides the highest peak at the fixed point (part of it serves as IOID), $\overline{\mathcal{W}}$ is also peaked to some lower heights along several other classical short periodic orbits that occur on the Wigner lat-

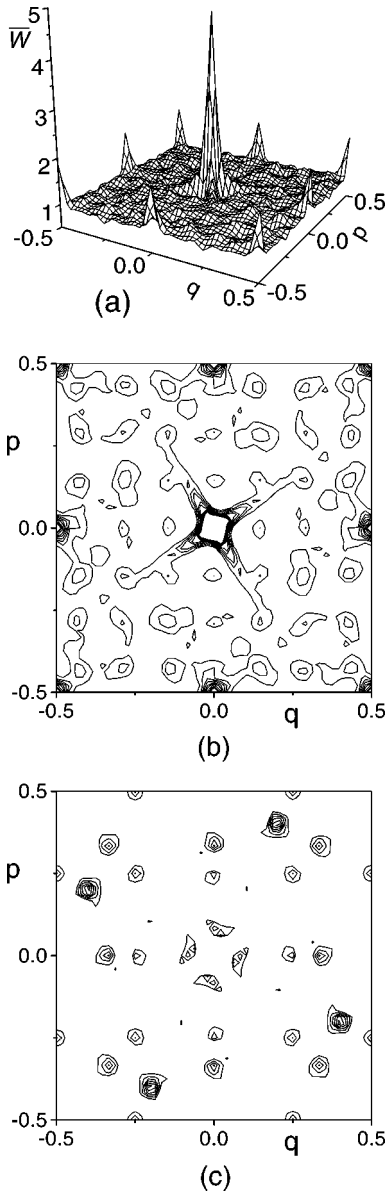

FIG. 5. (a) Three-dimensional plot of $\overline{\mathcal{W}}$ for $N=686$ [$\alpha(N)=1176$]. The IGD is at (0,0) with $a=0.024$ and $\epsilon=0.021$. Its contours ranging from 1 to 1.6 with step size 0.075 are shown in (b) and those from 0.73 to 0.92 with step size 0.0317 in (c).

tice. In Fig. 5(b), we plot the contours of $\overline{\mathcal{W}}$ ranging from 1 to 1.6, which shows these scars clearly. From this plot, one can recognize two groups of periodic orbits, one containing the period-3 orbit O_1 that strongly scars $\overline{\mathcal{W}}$ and the other one containing six period-8 orbits that scar $\overline{\mathcal{W}}$ relatively weakly. Together with the fixed point, the former forms the invariant sublattice I_1 and the latter forms I_2 [see Fig. 4(a)], and in each sublattice it seems the scars along those orbits that share the same period have the same height. This striking phenomenon, in which the periodic orbits scarring $\overline{\mathcal{W}}$ are organized into invariant sublattices of the Wigner lattice, is also observed for all other values of N that were investigated, and therefore it is believed to be a general feature.

A careful observation of the numerical data reveals that $\overline{\mathcal{W}}$ also takes the minima around some classical short periodic orbits. These valleys are known as antiscars for quantum eigenstates [9]. Because the absolute value of $\Delta\overline{\mathcal{W}}$ is usually quite small for $\overline{\mathcal{W}}<1$, we have to show these antiscars specifically. In Fig. 5(c), the contours of $\overline{\mathcal{W}}$ from its minimum to near 1 ($0.73-0.92$) are shown, and from it one can recognize the antiscarred periodic orbits almost at first sight (the minima on the middle lines between the stable and unstable manifolds of the fixed point should be regarded as part of IOID). According to the depth of the antiscars generated, they can be roughly classified into three groups: two period-2, two period-4, and four period-3 orbits [compare with Fig. 4(b)]. An interesting fact is that none of these orbits lives on the Wigner lattice at the present value of N. This is also a general feature.

One may notice that the fixed point is the common element of all sublattices of the Wigner lattice. So it is reasonable to conjecture that some of these sublattices being scarred in the above case may have a close connection with the fact that the IGD is actually placed on one of their points. This conjecture can be easily tested by checking whether or not a scarred sublattice will survive if the IGD is shifted to the other points. The answer is positive. As an example, we keep the other conditions used in Fig. 5 unchanged but shift the centroid of the IGD to (2/7,2/7) of a period-8 orbit in I_2 and plot the contours of $\overline{\mathcal{W}}$ in Fig. 6(a). We find that apart from IOID, the whole invariant sublattice I_2 generates scars again. An evident difference of Fig. 6(a) compared with Fig. 5(b) is that the scarred sublattice I_1 that once appeared in the latter now vanishes. Based on the above conjecture, one can attribute this to the fact that the IGD in this situation is quite apart from the I_1 sublattice. On the contrary, if the IGD sits on O_1, then I_1 (but not I_2) will be expected to be scarred instead. This has been easily verified by numerical calculation.

It is also of great interest to know what will happen if the IGD is shifted to the short periodic orbits that would antiscar $\overline{\mathcal{W}}$ when it is centered at the fixed point. Since these periodic orbits actually do not belong to the Wigner lattice, the way they act on $\overline{\mathcal{W}}$ must be different from that presented in the above paragraphs. A general simple rule is also found under this condition from extensive numerical investigations. As an illustration, the reader is referred to Fig. 6(b), where the contours of $\overline{\mathcal{W}}$ for the IGD being set at (1/3,1/3) of a period-4 orbit, which has been recognized from the antiscars of $\overline{\mathcal{W}}$ in Fig. 5(c), are presented. In addition to the IOID along this period-4 orbit, there is an accompanying period-12 orbit that weakly scars $\overline{\mathcal{W}}$. An interesting correlation between these two scarred orbits is that their relative position in phase space is the same as that of the fixed point and periodic orbit O_1 (which forms the invariant sublattice I_1). In other words, the points of the accompanying period-12 orbit can be divided into four groups; the three points in each group together with another one coming from the period-4 orbit can form a square of the same size of I_1. We find that this connection is not changed when the IGD is moved to the other

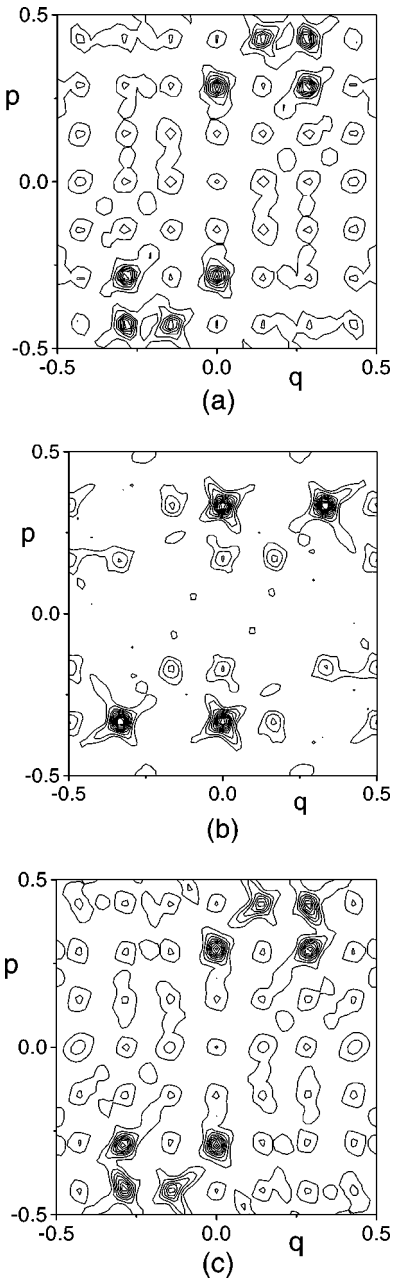

FIG. 6. Contours of $\overline{\mathcal{W}}$ for $N=686$, $a=0.024$, and $\epsilon=0.021$ with the IGD at (a) (2/7,2/7) (1 to 1.6 and 0.075 spaced), (b) (1/3,1/3) (1 to 1.7, 0.077 spaced), and (c) $(2/7+\Delta q, 2/7+\Delta p)$ with $\Delta q=\Delta p=0.01$ (1 to 1.5 and 0.063 spaced).

short periodic orbit that lives in the meshes of the Wigner lattice.

As a brief summary of this subsection, the short periodic orbits can be classified into different sets. Each set will generate scars simultaneously when the IGD is located on one of its points. We have two distinctive categories of these sets. Those in the first category can be identified with the invariant sublattices of the Wigner lattice, and those in the second category contain two short periodic orbits coupled through a square. A common important feature of all of these sets is that they have a certain stability when they are scarred. That means that even if the IGD is not set on them exactly, they can still manifest themselves clearly [Fig. 6(c)]. In fact, as the IGD is gradually moved away from one point of such a set, say a scarred invariant sublattice, one may find that in the first stage this scarred sublattice will survive well but the heights of the scars on it usually decrease. If another set is approached by the IGD during this process, then at the end $\overline{\mathcal{W}}$ will be taken over by the approached one. As to the intermediate states, sometimes a strong competition between the two opponents can occur so that it is difficult to recognize any one of them from the mingled structures of $\overline{\mathcal{W}}$. In spite of such a complication, these sets can serve perfectly as the backbones of the scars of $\overline{\mathcal{W}}$ in general cases, and therefore they are of great importance for studying the features of the phase-space structures resulting from the quantum coherence of the cat map.

Finally, it should be noted that, changing the parameters ϵ and a usually alters the sizes of the scars, antiscars, and IOID. If their values are decreased, finer scars and antiscars for longer periodic orbits usually will emerge, but no fresh clues have been deduced from them as to the ways in which they are organized.

VI. DISCUSSION

One of the unexpected results in our numerical investigations on the phase-space scars is that scarring for the quantum cat map appears not to be an individual behavior of a single orbit, but rather a collective one arising from some related short periodic orbits. Since the invariant sublattices for a given $N\times N$ Wigner lattice depend strongly on the number-theoretical nature of N, it is natural to expect that the time-averaged ensemble distribution $\overline{\mathcal{W}}(q,p)$ closely related to the invariant sublattices will do so as well.

On the other hand, from Eq. (4.8) we see that the QCE gives an overall measure of the deviation of $\mathcal{W}(q,p)$ from the uniform distribution. Thus corresponding to each dip in the time curve of S_ϵ (Fig. 2), there must be a strong localization in the time evolution of $\mathcal{W}(q,p)$. As a result, the decreasing of the time-averaged difference of QCE as N is increased (Table I) implies that $\Delta\overline{\mathcal{W}}(q,p)$ should vanish gradually as the semiclassical limit is approached. In order to get rid of the peculiar number-theoretical dependence of $\overline{\mathcal{W}}(q,p)$ on N, we can again restrict ourselves to the sequence of N, i.e., $N_l=N_0b^l, l=1,2,\ldots$ with b a prime, as we did in the preceding section. In Table I, the values of $\Delta\overline{\mathcal{W}}_{N_l}(q,p)$ at three different representative phase points for a sequence of N_l are shown. The numerical results show excellently that in the semiclassical regime

$$\Delta\overline{\mathcal{W}}_{N_{l+1}}(q,p)\approx\frac{1}{b}\Delta\overline{\mathcal{W}}_{N_l}(q,p), \tag{6.1}$$

i.e., the intensities of both the quantum scars (antiscars) and the IOID decrease linearly with the Planck constant for the cat map. It should be noted that the result obtained here does not contradict the common opinion that the intensities of the scars exhibited in the eigenstates of a chaotic system can be determined by classical dynamics and therefore should be

independent of the Planck constant [26]. In fact, in this paper, the semiclassical limit is implemented with a fixed initial phase-space distribution, which should be described by different density operators when the Planck constant is changed. We think that in order to get some physical insights into the semiclassical limiting properties, it is important to consider a fixed physical state rather than a fixed mathematical state.

Since, up to now, most efforts on scars have concentrated on the study of energy eigenstates, an interesting question that remains to be answered is the relationship between the scars we have observed in the time-averaged ensemble distribution of the quantum cat map and those exhibited in its quasienergy eigenstates. Here is a simple calculation that gives the answer.

Let $|\phi_r\rangle, r=1,\ldots,N$ be a complete set of the quasienergy eigenstates of the time evolution operator $\hat{S}$, and let $e^{i\theta_r}, r=1,\ldots,N$ be the corresponding eigenvalues. Then the eigenangle θ_r can only take one of the following $\alpha(N)$ possible values:

$$\beta_u=\frac{2\pi u+\gamma_N}{\alpha(N)}, \quad u=1,\ldots,\alpha(N), \tag{6.2}$$

where γ_N is a constant that depends only on N [16]. Now, for any given initial ensemble distribution, one can always construct an orthogonal set of quasienergy eigenstates $|\phi_r\rangle, r=1,\ldots,N'$ $(N'\leqslant N)$ with distinct eigenangles θ_r such that its density operator has the form

$$\hat{\rho}^0=\sum_{r,s=1}^{N'} \rho^0_{rs}|\phi_r\rangle\langle\phi_s|. \tag{6.3}$$

By making use of Eq. (2.4), the time-averaged density operator can be expressed as

$$\overline{\hat{\rho}}=\frac{1}{\alpha(N)}\sum_{k=0}^{\alpha(N)-1}\hat{\rho}^k=\sum_{r=1}^{N'}\rho^0_{rr}|\phi_r\rangle\langle\phi_r|, \tag{6.4}$$

from which we have

$$\overline{W}(q_j,p_l)=\sum_{r=1}^{N'}\langle\phi_r|\hat{\rho}^0|\phi_r\rangle W_r(q_j,p_l) \tag{6.5}$$

by straightforward application of Eq. (3.2). Here $W_r(q_j,p_l)$ denotes the Wigner function of the eigenstate $|\phi_r\rangle$. It tells that $\overline{W}(q_j,p_l)$ is just a linear combination of the Wigner functions of the eigenstates. As a result, the scars caused by the classical short periodic orbits on each eigenfunction will accumulate to form the structures of $\overline{\mathcal{W}}(q,p)$, which we have shown in our figures.

VII. SUMMARY

We have presented a detailed study of the quantum motion of an ensemble of Arnold's cat map in the context of statistical mechanics. By investigating the evolution of the quantum ensembles, we found that quantum coherence manifests itself through an irregular sequence of dips in the time curve of coarse-grained entropy after the system reaches the transient equilibrium state. Moreover, we find that the deviation of the time average of the quantum coarse-grained entropy from its classical counterpart decreases linearly with $\hbar$ when the semiclassical limit is taken by letting $\hbar=1/(2\pi N_0 b^l)$ with b a prime and $l\to\infty$.

Meanwhile, we find that classical short periodic orbits have strong influences on the time-averaged Wigner function by scarring and antiscarring the latter. (Although antiscars have been predicted theoretically in Ozorio de Almeida's book [9], reports on its direct observation are rare in publications, so our observation provides numerical evidence.) Furthermore, these short periodic orbits usually occur in sets rather than individually. Finally, we have shown that the deviation of the time average of the coarse-grained Wigner function from its classical counterpart also decreases linearly with $\hbar$ in the semiclassical regime along the above-mentioned sequence of $\hbar$.

ACKNOWLEDGMENT

J.W. is supported by the National Science and Technology Board, Singapore.

[1] A. I. Schnirelman, Usp. Mat. Nauk **29**, 181 (1974); Y. Colin de Verdiere, Commun. Math. Phys. **102**, 497 (1985); S. Zelditch, Duke Math. J. **55**, 919 (1987).
[2] B. Eckhardt *et al.*, Phys. Rev. E **52**, 5893 (1995).
[3] O. Bohigas, M.-J. Giannoni, and C. Schmit, J. Phys. (Paris) Lett. **45**, L1015 (1984).
[4] M. L. Mehta, *Random Matrices* (Academic Press, New York, 1991); F. Haake, *Quantum Signatures of Chaos* (Springer-Verlag, Berlin, 1992).
[5] L. Kaplan and E. J. Heller, Physica D **121**, 1 (1984); S. Zelditch, *ibid.* **121**, 19 (1984).
[6] M. C. Gutzwiller, *Chaos in Classical and Quantum Mechanics* (Springer-Verlag, New York, 1992).
[7] E. J. Heller, Phys. Rev. Lett. **53**, 1515 (1984).
[8] L. Kaplan, Nonlinearity **12**, R1 (1999).
[9] A. M. Ozorio de Almeida, *Hamiltonian Systems: Chaos and Quantization* (Cambridge University Press, Cambridge, UK, 1988).
[10] V. I. Arnold and A. Avez, *Ergodic Problems of Classical Mechanics* (Benjamin, New York, 1968).
[11] Y. Gu, Phys. Rev. A **32**, 1310 (1985).
[12] Y. Gu, Phys. Lett. A **149**, 95 (1990).
[13] Y. Gu and J. Wang, Phys. Lett. A **229**, 208 (1997).
[14] G. Casati, B. V. Chirikov, F. M. Izrailev, and J. Ford, Lect. Notes Phys. **93**, 334 (1979); F. M. Izrailev, Phys. Rep. **196**, 299 (1990).
[15] B. V. Chirikov, in *Chaos and Quantum Physics*, edited by M. J. Giannoni, A. Voros, and J. Zinn-Justin (Elsevier, Amsterdam, 1990), p. 443.
[16] J. H. Hannay and M. V. Berry, Physica D **1**, 267 (1980).

[17] N. L. Balazs and A. Voros, Ann. Phys. (N.Y.) **190**, 1 (1989).
[18] J. Ford, G. Mantica, and G. H. Ristow, Physica D **50**, 493 (1991).
[19] J. M. Jauch, in *The Physicist's Conception of Nature*, edited by J. Mehra (Reidel, Dordrecht, 1973), p. 300.
[20] J. P. Keating, Nonlinearity **4**, 277 (1991); **4**, 309 (1991).
[21] M. V. Berry and N. L. Balazs, J. Phys. A **12**, 625 (1979).
[22] S. J. Chang and K. J. Shi, Phys. Rev. Lett. **55**, 269 (1985); Phys. Rev. A **34**, 7 (1986).
[23] I. Prigogine, in *The Physicist's Conception of Nature* (Ref. [19]), p. 579.
[24] R. L. Waterland, J. M. Yuan, C. C. Martens, R. E. Gillilan, and W. P. Reinhardt, Phys. Rev. Lett. **61**, 2733 (1988).
[25] I. Percival and F. Vivaldi, Physica D **25**, 105 (1987).
[26] E.J. Heller, in *Chaos and Quantum Physics* (Ref. [15]), p. 547.